

# Diversity of chain, interwoven and network structures formed by metal complexes with 2,3,5,6-tetrafluoro-1,4-bis(4-pyridylsulfenyl)benzene †

David M. L. Goodgame,\* David A. Grachvogel, Stephanie Holland, Nicholas J. Long, Andrew J. P. White and David J. Williams\*

Department of Chemistry, Imperial College of Science, Technology and Medicine, London, UK SW7 2AY

Received 4th June 1999, Accepted 22nd July 1999

The preparations are reported of a range of complexes formed by 2,3,5,6-tetrafluoro-1,4-bis(4-pyridylsulfenyl)benzene (L) with  $Mn^{II}$ ,  $Co^{II}$ ,  $Ni^{II}$ ,  $Zn^{II}$  and  $Cd^{II}$ , and single crystal X-ray diffraction studies have been made on four of the compounds. In the complex  $CoL_2 \cdot 0.5CH_2Cl_2$ , the organic ligand bridges tetrahedrally coordinated  $Co^{II}$  centres so as to form chains. The compound  $Cd_2L_3(NO_3)_4$  has a more complex structure in which seven-coordinate Cd centres are linked by two different types of L bridges so as to form arrays of 90-membered macrocycles comprising sheets of linked alternating enantiomeric helices. In the complexes  $MnL_2(EtOH)_2X_2$  ( $X = Br$  or  $NCS$ ), the bis(pyridyl) ligand utilises only one of its pyridyl units to coordinate directly to the metal atom. In both cases the Mn coordination environment comprises an all-*trans* octahedral arrangement of two anions, two ethanol ligands and two pyridyl units derived from two different L ligands. However in both compounds the non-coordinated pyridyl units bridge adjacent Mn centres by forming hydrogen bonds to the ethanol ligands. The resulting, complex networks are, however, dramatically different. The isothiocyanate complex forms sheets of partially interpenetrating helices whereas the bromide forms a system of triply interpenetrating (4,4) nets of 'over 2-under 2' type. X- and Q-Band EPR spectra of the manganese complexes are reported as are relevant spectroscopic results for the other complexes.

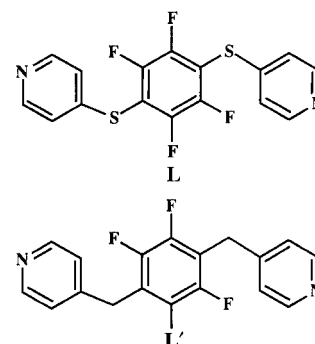
## Introduction

Over the past decade there has been a resurgence of interest in the construction of coordination polymers with a view to synthesising new materials with controllable physical properties.<sup>1</sup> Workers in this field have given much attention to the use of 4,4'-bipyridyl as the connecting ligand to form molecular squares and more extended networks;<sup>2</sup> similarly use of ligands in which pairs of 4-pyridyl units are linked by a variety of spacer groups has also proved to be a very fruitful approach to the formation of a range of polymeric structures.<sup>3-5</sup> As part of our continued interest in the formation of new coordination polymers, we recently reported the structures and EPR spectra of chain polymeric complexes of copper(II) chloride and bromide with the 'extended reach' ligand 2,3,5,6-tetrafluoro-1,4-bis(4-pyridylsulfenyl)benzene, L, and its 2-pyridylsulfenyl analogue.<sup>6</sup> As it appeared that ligand L had significant potential for the generation of more complex coordination polymeric networks by changing the preferred coordination geometry at the metal centres and particularly to those which favour octahedral coordination, we extended our studies to a wider range of metal ions of the First Transition Series and also to cadmium(II). This has resulted in the formation of four different types of unusual network structures which we report here together with the spectroscopic properties of some other new complexes formed by L.

## Experimental

### Preparations

**2,3,5,6-Tetrafluoro-1,4-bis(4-pyridylsulfenyl)benzene (L).** This was obtained as described previously.<sup>6</sup>



**Metal complexes.** The complexes obtained are listed in Table 1, together with the product yields and their analytical data (Scientific Analysis and Consultancy Service, University of North London).

Unless stated otherwise below, the standard method of preparation employed was to place a solution of 2,3,5,6-tetrafluoro-1,4-bis(4-pyridylsulfenyl)benzene (0.068 mmol) in dichloromethane (3 cm<sup>3</sup>) in a test-tube and then carefully 'layer' onto it firstly ethanol (1 cm<sup>3</sup>) and then a solution of the appropriate metal salt (0.034 mmol) in ethanol (3 cm<sup>3</sup>). The test-tube was then sealed and left to stand at room temperature for several days. The solid product was filtered off, washed with diethyl ether and air-dried.

*MnLCl<sub>2</sub> 1.* Standard method using  $MnCl_2 \cdot 4H_2O$ .

*MnL<sub>2</sub>Cl<sub>2</sub> 2.* A solution of anhydrous  $MnCl_2$  (0.034 mmol) in a 1:1 mixture of ethanol and 2,2-dimethoxypropane (3 cm<sup>3</sup>) was carefully 'layered' on the top of a solution of ligand L (0.068 mmol) also in 1:1 ethanol-2,2-dimethoxypropane (3 cm<sup>3</sup>) in a test-tube. After 8 days the solid product which had formed was filtered off, washed with diethyl ether and air-dried.

† Supplementary data available: rotatable 3-D crystal structure diagram in CHIME format. See <http://www.rsc.org/suppdata/dt/1999/3473/>

**Table 1** Microanalytical data for complexes of 2,3,5,6-tetrafluoro-1,4-bis(4-pyridylsulfenyl)benzene (L)

Complex	Colour	Yield (%)	Analysis (%) <sup>a</sup>		
			C	H	N
1 MnLCl <sub>2</sub>	White	71	38.3 (38.9)	1.6 (1.6)	5.7 (5.7)
2 MnL <sub>2</sub> Cl <sub>2</sub>	White	68	44.7 (44.6)	2.1 (1.9)	6.7 (6.5)
3 [MnL <sub>2</sub> (EtOH) <sub>2</sub> Br <sub>2</sub> ]	Colourless	73	41.8 (41.4)	2.3 (2.7)	5.5 (5.4)
4 [MnL <sub>2</sub> (EtOH) <sub>2</sub> (NCS) <sub>2</sub> ]	Colourless	77	45.7 (45.7)	2.9 (2.8)	8.3 (8.4)
5 CoLCl <sub>2</sub>	Bright blue	83	38.3 (38.6)	1.4 (1.6)	5.6 (5.6)
6 CoLI <sub>2</sub>	Green-blue	52	28.6 (28.2)	1.3 (1.2)	4.3 (4.1)
7 NiLCl <sub>2</sub>	Pale green	65	38.5 (38.6)	1.7 (1.6)	5.5 (5.6)
8 ZnLCl <sub>2</sub>	White	88	38.2 (38.1)	1.3 (1.6)	5.3 (5.6)
9 ZnLBr <sub>2</sub>	White	69	32.8 (32.4)	1.4 (1.4)	4.5 (4.7)
10 ZnLI <sub>2</sub>	White	88	27.6 (28.0)	1.1 (1.2)	4.0 (4.1)
11 ZnL(NO <sub>3</sub> ) <sub>2</sub>	Colourless	79	34.7 (34.5)	1.4 (1.5)	10.0 (10.0)
12 CdLCl <sub>2</sub>	White	69	34.4 (34.8)	1.7 (1.5)	4.8 (5.1)
13 CdLBr <sub>2</sub>	White	97	30.0 (30.0)	1.1 (1.3)	4.5 (4.4)
14 CdLI <sub>2</sub>	Colourless	80	26.4 (26.2)	0.9 (1.1)	3.8 (3.8)
15 Cd <sub>2</sub> L <sub>3</sub> (NO <sub>3</sub> ) <sub>4</sub>	Colourless	61	36.7 (36.5)	1.5 (1.5)	8.8 (8.9)

<sup>a</sup> Calculated value in parentheses.**Table 2** Crystal data and summary of data collection and refinement for compounds **3**, **4**, **6** and **15**

	<b>3</b>	<b>4</b>	<b>6</b>	<b>15</b>
Formula	C <sub>36</sub> H <sub>28</sub> F <sub>8</sub> Br <sub>2</sub> MnN <sub>4</sub> O <sub>2</sub> S <sub>4</sub>	C <sub>38</sub> H <sub>28</sub> F <sub>8</sub> MnN <sub>6</sub> O <sub>2</sub> S <sub>6</sub>	C <sub>16</sub> H <sub>8</sub> CoF <sub>4</sub> N <sub>2</sub> I <sub>2</sub> S <sub>2</sub> ·0.5CH <sub>2</sub> Cl <sub>2</sub>	C <sub>24</sub> H <sub>12</sub> CdF <sub>6</sub> N <sub>5</sub> O <sub>6</sub> S <sub>3</sub> ·CH <sub>2</sub> Cl <sub>2</sub>
<i>M</i>	1043.6	1000.0	723.6	873.9
Crystal system	Orthorhombic	Monoclinic	Monoclinic	Monoclinic
Space group	<i>Pna</i> 2 <sub>1</sub> (no. 33)	<i>P</i> 2 <sub>1</sub> / <i>c</i> (no. 14)	<i>P</i> 2 <sub>1</sub> / <i>c</i> (no. 14)	<i>C</i> 2/ <i>c</i> (no. 15)
<i>a</i> /Å	14.744(1)	15.102(1)	5.988(2)	28.714(3)
<i>b</i> /Å	9.644(1)	7.783(1)	16.777(3)	8.244(1)
<i>c</i> /Å	27.253(2)	18.025(3)	23.539(3)	28.736(3)
$\beta$ /°	—	101.45(1)	96.29(2)	96.63(1)
<i>U</i> /Å <sup>3</sup>	3875.0(7)	2076.6(4)	2350.6(8)	6757(2)
<i>Z</i>	4	2 <sup>a</sup>	4	8
$\mu$ /mm <sup>-1</sup>	7.91	6.11	3.69	9.10
<i>T</i> /K	293	293	293	293
Unique reflections:				
measured ( <i>R</i> <sub>int</sub> )	2804 (0.00)	3079 (0.03)	4123 (0.03)	5323 (0.04)
observed, $ F_o  > 4\sigma( F_o )$	2144	2104	2906	3967
<i>R</i> <sub>1</sub> , <i>wR</i> <sub>2</sub> <sup>b</sup>	0.058, 0.131	0.070, 0.171	0.056, 0.135	0.052, 0.124

<sup>a</sup> The molecule has crystallographic C<sub>i</sub> symmetry. <sup>b</sup>  $R_1 = \sum[|F_o| - |F_c|]/\sum|F_o|$ ;  $wR_2 = [\sum w(F_o^2 - F_c^2)^2/\sum w(F_o^2)]^{1/2}$ ;  $w^{-1} = \sigma^2(F_o^2) + (aP)^2 + bP$ .

[MnL<sub>2</sub>(EtOH)<sub>2</sub>(NCS)<sub>2</sub>] **4**. Standard method but using L in chloroform (4 cm<sup>3</sup>) and Mn(NCS)<sub>2</sub> (0.034 mmol) in ethanol (4 cm<sup>3</sup>).

### Physical measurements

Electronic spectra were obtained on powdered samples by the reflectance method using a Beckmann DK2 spectrometer. IR spectra were measured as CsI pressed discs using a Mattson Polaris FTIR spectrometer. Raman spectra were recorded on a Perkin Elmer 1720 FT instrument with Nd–YAG laser excitation and also using a Dilors Labram Infinity instrument with He–Ne (633 nm) and a frequency doubled Nd–YAG (532 nm) laser.

EPR spectra were obtained for powdered samples at room temperature on a Varian E12 X-band spectrometer. EPR spectra for compounds **2–4** were also obtained at the EPSRC. cw-EPR Service Centre, Department of Chemistry, University of Manchester at both X- and Q-band frequencies on a Bruker ESP300E spectrometer. Magnetic fields and microwave frequencies were calibrated with a Bruker ER035M NMR gaussmeter and an EIP model 588C microwave pulse counter, respectively.

### X-Ray crystallography

A summary of the crystal data and of the data collection and refinement parameters for compounds **3**, **4**, **6** and **15** is given in Table 2. Data were collected at room temperature on a Siemens P4/PC diffractometer using graphite-monochromated Cu–K $\alpha$

radiation for **3**, **4** and **15** and Mo–K $\alpha$  for **6**, in each case using  $\omega$  scans. The data were corrected for Lorentz and polarisation effects and for absorption (lamina [001] for **3** and ellipsoidal for **4**, **6** and **15**).

The structures of **3**, **4** and **6** were solved by direct methods and that of **15** by the heavy atom method, and they were all refined by full matrix least-squares based on *F*<sup>2</sup>. In **4** disorder was found in the ethyl portion of the coordinated ethanol molecule and in **15** disorder was present in the dichloromethane solvent molecule; in each case two partial occupancy orientations were identified and refined anisotropically. The remaining non-hydrogen atoms in all four structures were refined anisotropically. The C–H hydrogen atoms in all four structures were placed in calculated positions, assigned isotropic thermal parameters,  $U(\text{H}) = 1.2U_{\text{eq}}(\text{C})$ , [ $U(\text{H}) = 1.5U_{\text{eq}}(\text{C–Me})$ ], and allowed to ride on their parent atoms. The O–H hydrogen atom in **4** was located from a  $\Delta F$  map and refined isotropically subject to a distance constraint (0.90 Å); those in **3** could not be located. The polarity of **3** could not be unambiguously determined. All computations were carried out using the SHELXTL PC program system.<sup>7</sup> Bond lengths and angles for **3**, **4**, **6** and **15** are given in Tables 3–6 respectively.

The X-ray powder diffraction studies were carried out using a Siemens D500 powder diffractometer operating in reflecting mode with a diffracted beam monochromator.

CCDC reference number 186/1596.

See <http://www.rsc.org/suppdata/dt/1999/3473/> for crystallographic files in .cif format.

**Table 3** Selected bond lengths (Å) and angles (°) for compound **3**

Mn–O(50)	2.216(12)	Mn–O(60)	2.215(12)
Mn–N(1)	2.317(13)	Mn–N(21)	2.315(13)
Mn–Br(2)	2.677(3)	Mn–Br(1)	2.681(3)
O(60)–Mn–O(50)	179.5(6)	O(60)–Mn–N(1)	91.3(5)
O(50)–Mn–N(1)	88.7(5)	O(60)–Mn–N(21)	89.5(5)
O(50)–Mn–N(21)	90.5(5)	N(1)–Mn–N(21)	178.9(6)
O(60)–Mn–Br(2)	94.0(3)	O(50)–Mn–Br(2)	85.5(3)
N(1)–Mn–Br(2)	89.8(4)	N(21)–Mn–Br(2)	90.9(4)
O(60)–Mn–Br(1)	85.8(3)	O(50)–Mn–Br(1)	94.7(3)
N(1)–Mn–Br(1)	90.6(3)	N(21)–Mn–Br(1)	88.7(4)
Br(1)–Mn–Br(2)	179.6(2)		

**Table 4** Selected bond lengths (Å) and angles (°) for compound **4**

Mn–N(1)	2.318(5)	Mn–N(21)	2.149(6)
Mn–O(30)	2.256(5)		
N(21)–Mn–N(21A)	180.0	N(21)–Mn–O(30)	90.9(2)
N(21A)–Mn–O(30)	89.1(2)	O(30)–Mn–O(30A)	180.0
N(21)–Mn–N(1A)	89.4(2)	N(21)–Mn–N(1)	90.6(2)
O(30)–Mn–N(1A)	84.7(2)	O(30)–Mn–N(1)	95.3(2)
N(1)–Mn–N(1A)	180.0		

**Table 5** Selected bond lengths (Å) and angles (°) for compound **6**

Co–N(1)	2.037(7)	Co–N(18A)	2.044(8)
Co–I(1)	2.5796(14)	Co–I(2)	2.5747(13)
N(1)–Co–N(18A)	108.8(3)	N(1)–Co–I(1)	105.2(2)
N(18A)–Co–I(1)	104.7(2)	N(1)–Co–I(2)	108.7(2)
N(18A)–Co–I(2)	108.0(2)	I(1)–Co–I(2)	121.01(6)

**Table 6** Selected bond lengths (Å) and angles (°) for compound **15**

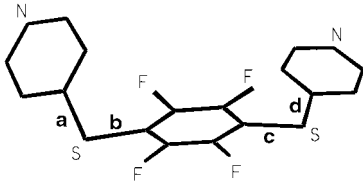
Cd–N(1)	2.329(5)	Cd–N(11)	2.317(6)
Cd–N(21)	2.309(6)	Cd–O(40)	2.474(6)
Cd–O(41)	2.399(6)	Cd–O(50)	2.459(5)
Cd–O(51)	2.434(6)		
N(21)–Cd–N(11)	106.7(2)	N(21)–Cd–N(1)	94.7(2)
N(11)–Cd–N(1)	157.4(2)	N(21)–Cd–O(41)	84.5(2)
N(11)–Cd–O(41)	84.2(2)	N(1)–Cd–O(41)	90.7(2)
N(21)–Cd–O(51)	85.3(2)	N(11)–Cd–O(51)	86.4(2)
N(1)–Cd–O(51)	103.0(2)	O(41)–Cd–O(51)	163.5(2)
N(21)–Cd–O(50)	134.8(2)	N(11)–Cd–O(50)	87.1(2)
N(1)–Cd–O(50)	82.9(2)	O(41)–Cd–O(50)	140.4(2)
O(51)–Cd–O(50)	52.1(2)	N(21)–Cd–O(40)	136.5(2)
N(11)–Cd–O(40)	78.5(2)	N(1)–Cd–O(40)	80.9(2)
O(41)–Cd–O(40)	52.6(2)	O(51)–Cd–O(40)	138.0(2)
O(50)–Cd–O(40)	87.8(2)		

## Results and discussion

As our main objective was a study of the ability of ligand **L** to form polymeric arrays with metal ions we have concentrated on attempts to obtain crystalline complexes suitable for single-crystal X-ray analysis. Of the new compounds listed in Table 1, good crystals were obtained for compounds **3**, **4**, **6** and **15**, and we shall describe their structures in order of increasing complexity and then discuss such additional information as may be derived from the spectroscopic studies both on these compounds and also the other complexes for which full X-ray characterisation was not achieved.

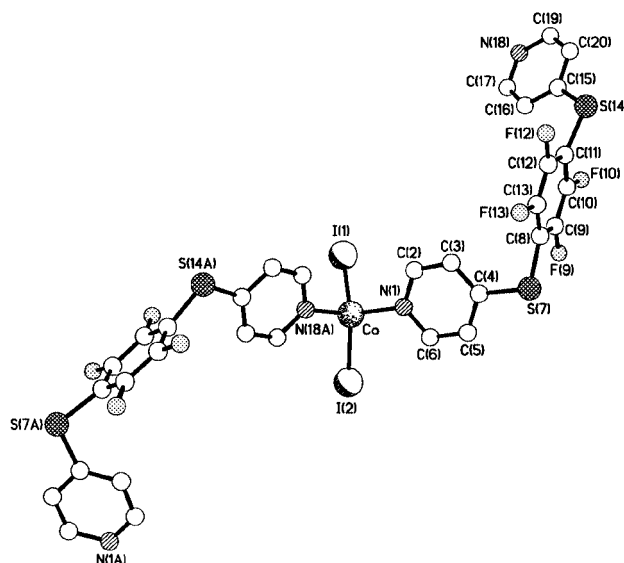
### Structure of $\text{CoLi}_2 \cdot 0.5\text{CH}_2\text{Cl}_2$ , $\text{6} \cdot 0.5\text{CH}_2\text{Cl}_2$

The crystal structure study on complex **6** shows that the 2,3,5,6-tetrafluoro-1,4-bis(4-pyridylsulfenyl)benzene ligand links adjacent tetrahedrally coordinated cobalt centres to form continuous, sinuous polymeric chains that propagate along the

**Table 7** Comparative torsional relationships (°) between the pyridyl and  $\text{C}_6\text{F}_4$  rings in compounds **3**, **4**, **6** and **15**


	<b>3<sup>a</sup></b>	<b>3<sup>b</sup></b>	<b>4<sup>c</sup></b>	<b>6<sup>d</sup></b>	<b>15<sup>e</sup></b>	<b>15<sup>f</sup></b>
<b>a</b>	24	22	18	27	47	9
<b>b</b>	70	68	90	83	84	65
<b>c</b>	82	85	72	62	80	65
<b>d</b>	23	23	29	4	15	9

<sup>a</sup> From N1 to N18 in Fig. 9. <sup>b</sup> From N21 to N38 in Fig. 9. <sup>c</sup> From N1 to N18 in Fig. 6. <sup>d</sup> From N1 to N18 in Fig. 1. <sup>e</sup> From N11 to N21A in Fig. 3. <sup>f</sup> From N1 to N1A in Fig. 3.

**Fig. 1** The cobalt coordination environment in the structure of **6**.

crystallographic *b* direction. The tetrahedral geometry at Co is significantly distorted (Fig. 1), the I–Co–I angle being enlarged to 121.0(1)° whilst the N–Co–N angle is close to tetrahedral at 108.8(3)°; the coordination bond lengths are unexceptional (Table 5).

The bis(pyridyl) ligand has a *syn* conformation, with the two pyridyl rings steeply inclined to the central  $\text{C}_6\text{F}_4$  unit (Table 7). As expected, there are significant enlargements of the angles at C(4) and C(15) [C(3)–C(4)–S(7) 124.2(8)° and S(14)–C(15)–C(16) 126.9(7)°] and concomitant contractions of C(5)–C(4)–S(7) [116.3(8)°] and S(14)–C(15)–C(20) [116.1(7)°] accompanying this conformation.<sup>6,8</sup> There is also a marked bowing of the S– $\text{C}_6\text{F}_4$ –S unit—the two S–C bonds subtending an angle of 13°.

Adjacent chains pack in register, creating small channels at the troughs and crests, within which the occluded dichloromethane solvent molecules are located (Fig. 2). Two interesting features of the packing of the polymer chains are: (1) a short (2.99 Å) and nearly orthogonal (82°) approach of one of the fluorine atoms in one chain to a pyridyl ring in the next, and (2) a pair of weak I⋯ $\pi$  interactions (3.97 Å) between I(1) and the  $\text{C}_6\text{F}_4$  ring (I⋯centroid vector inclined by 72°) and also between I(2) and the N(1)–C(6) pyridyl ring (3.99 Å to centroid; vector inclined by 84°). In this context, it is interesting to note that in the previously reported structure<sup>6</sup> of the chain-polymeric copper(II) bromide complex  $\{[\text{CuL}(\text{DMF})\text{Br}_2] \cdot (\text{DMF})\}_n$  formed by **L**, there are analogous Br⋯ $\text{C}_6\text{F}_4$  interactions with Br⋯ $\pi$  distances of 3.47 Å and 3.69 Å and angles

of approach of  $74^\circ$  in each case (for the former of these distances the Br atom lies only  $3.34 \text{ \AA}$  from the ring plane). It seems clear that these weak electrostatic interactions must influence the chain packing in the crystals of both **6** and the copper bromide complex  $\{[\text{CuL}(\text{DMF})\text{Br}_2] \cdot (\text{DMF})\}_n$ .

### Structure of $\text{Cd}_2\text{L}_3(\text{NO}_3)_4$ **15**

The structure of  $\text{Cd}_2\text{L}_3(\text{NO}_3)_4$ , **15**, shows that each cadmium atom is bonded to three 2,3,5,6-tetrafluoro-1,4-bis(4-pyridyl-sulfonyl)benzene ligands and to two chelating nitrates (Fig. 3). Each cadmium is formally seven-coordinate but if one considers each nitrate occupying a single coordination site the geometry can be regarded as either distorted trigonal bipyramidal [with N(1) and N(11) occupying the axial positions] or as distorted square pyramidal [with N(21) in the apical position]. This geometry at the metal centre is very similar to that observed<sup>4</sup> in the closely-related cadmium nitrate complex formed by the 2,3,5,6-tetrafluoro-1,4-bis(4-pyridylmethyl)-benzene ligand ( $\text{L}'$ ).

In compound **15** there are two different ligand conformations. One (**A** in Fig. 3) has a *syn* relationship between the two pyridyl ring systems, but with torsional relationships that differ from those in compound **6** (Table 7), whilst the other (**B** in Fig. 3) has a  $C_1$  symmetric *anti* conformation (which is the conformation adopted by all of the bis(pyridyl) ligands in  $\text{Cd}_2(\text{L}')_3(\text{NO}_3)_4$ ).<sup>4</sup> In **15** both ligand types bridge between adjacent metal centres but do so in two different ways. The linking by ligands

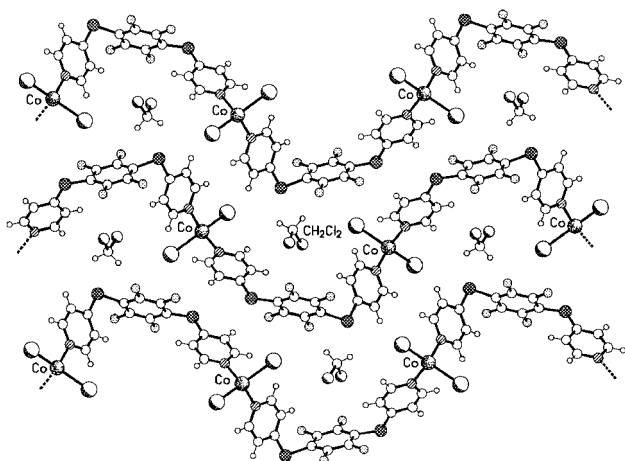


**Fig. 2** The sinusoidal chains formed by **6**, showing the siting of the dichloromethane solvent molecules that lie in the channels running normal to the plane of the paper.

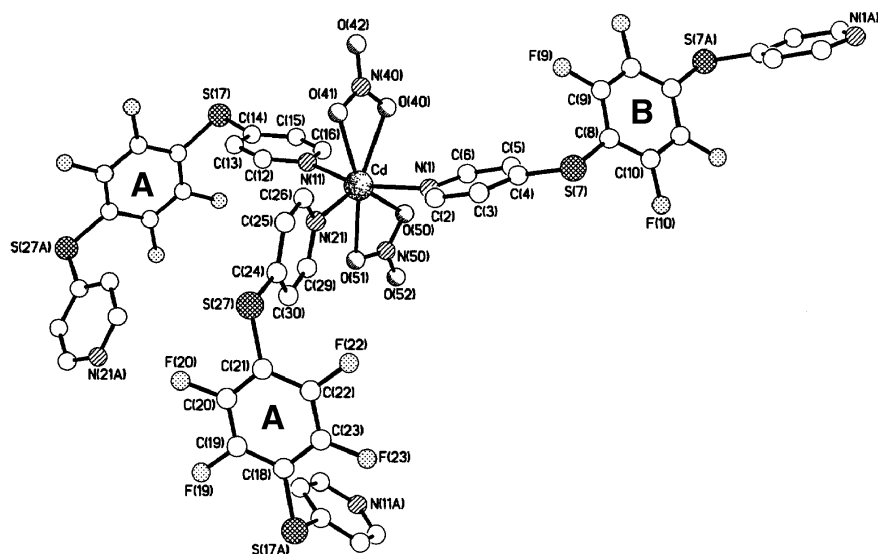


**Fig. 3** The cadmium coordination environment in the structure of **15**, also showing the two independent ligand conformations of types **A** and **B**.

of type **A** creates slightly flattened helices (Fig. 4) that extend along the crystallographic *b* direction. Those of type **B** cross-link adjacent helices to form continuous sheets of alternating

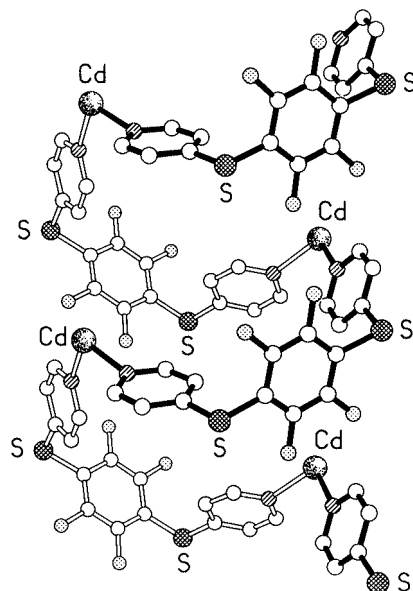


**Fig. 4** Part of one of the helical chains linking adjacent cadmium atoms in **15**.

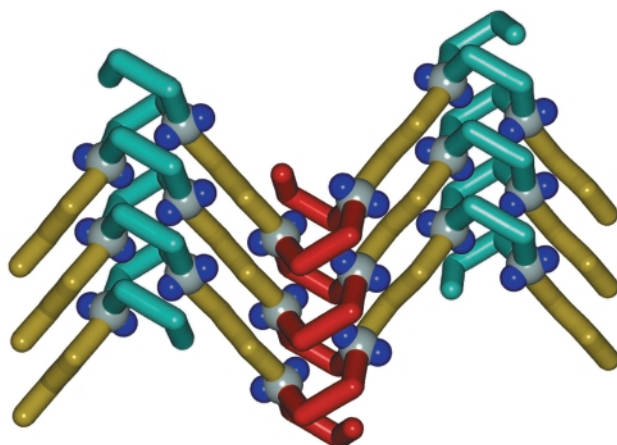


**Fig. 5** Schematic representation of the linking by ligands of type **B** (yellow) of adjacent enantiomeric (green-blue and red) helical chains in the structure of **15**.

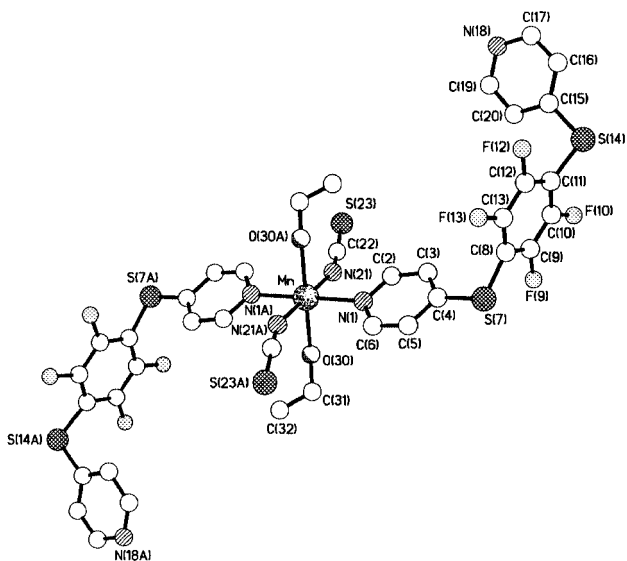


Fig. 6 The manganese coordination environment in the structure of **4**.

enantiomeric helices. This arrangement is depicted schematically in Fig. 5. This type **B** cross-linking, coupled with the 'two-ligand pitch' of each helix, creates contiguous arrays of 6-ligand 90-membered macrocycles. It is interesting to note that in the structure of  $\text{Cd}_2(\text{L}')_3(\text{NO}_3)_4$ ,<sup>4</sup> which does not contain helical linkages, analogous 6-ligand 90-membered macrocycles are also present. However, in the structure of  $\text{Cd}_2(\text{L}')_3(\text{NO}_3)_4$  a triply interpenetrating 2-D structure is observed which is not the case for **15**. The structure of **15** could alternatively be described as a 2-D, all-covalent network with (6,3) topology.

In **15** the only intra-sheet interaction of note is a very short dual approach (3.04 Å) of a pair of nitrate oxygen atoms from opposite sides to the centre of a  $\text{C}_6\text{F}_4$  ring of one of the cross-linking **B**-type ligands. Because of this observation we have analysed the published<sup>4</sup> crystallographic data for  $\text{Cd}_2(\text{L}')_3(\text{NO}_3)_4$  and find that it also contains analogous nitrate... $\text{C}_6\text{F}_4$  approaches, though in that case the distances are longer, the shortest being 3.22 Å (*cf.* 3.035 Å in **15**). The shortest inter-sheet contact in **15** is 3.34 Å between the same nitrate oxygen atom [O(42)] and the centre of the  $\text{C}_6\text{F}_4$  ring of an **A**-type ligand.

#### Structure of $[\text{MnL}_2(\text{EtOH})_2(\text{NCS})_2]$ **4**

In contrast to the structures of **6** and **15**, where the 2,3,5,6-tetrafluoro-1,4-bis(4-pyridylsulfenyl)benzene ligand is binucleating and utilises both pyridyl nitrogen atoms as coordination sites, in the structure of **4** only one of the nitrogen atoms of each ligand coordinates to the manganese. The coordination sphere of each manganese centre (Fig. 6) comprises two nitrogen atoms, one from each of two bis(pyridyl) ligands, the nitrogen atoms of the two isothiocyanate ligands and the oxygen atoms of two ethanol molecules, from the solvent used in the synthesis. Each ligand pair is disposed in *trans* orientation, the Mn atom lying on an inversion centre. The departures from octahedral geometry are relatively small, the *cis* angles ranging from 84.7(2) to 95.3(2)°. The Mn–N distances are 2.318(5) Å to the pyridyl nitrogen N(1) and 2.149(6) Å to the isothiocyanate nitrogen N(21); the Mn–O distances are 2.256(5) Å.

The bis(pyridyl) ligand has a *syn* conformation, the N(1) pyridyl ring being in an orthogonal relationship with respect to the  $\text{C}_6\text{F}_4$  ring whilst the other pyridyl ring is more skewed (Table 7). The orthogonal geometry is accompanied by a noticeable enlargement of the C(3)–C(4)–S(7) angle [124.9(5)°] and a marked bowing of the S– $\text{C}_6\text{F}_4$ –S unit, the two C–S bonds being mutually inclined by 15°.

Structural propagation analogous to that in compounds **6** and **15** still occurs but *via*  $\text{OH}\cdots\text{N}$  hydrogen bonding between

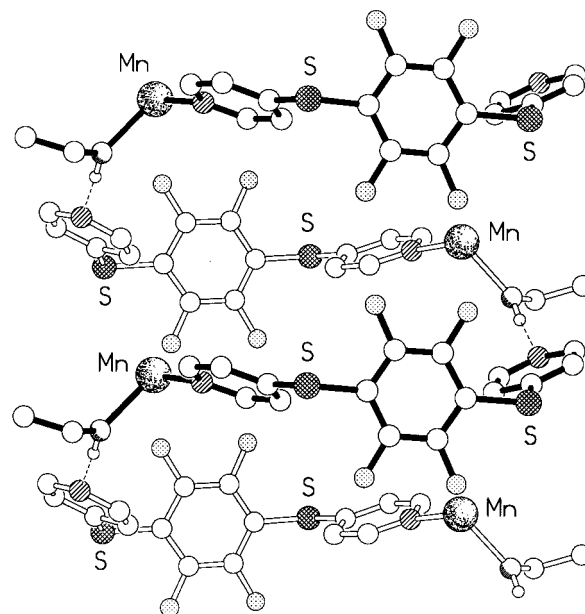


Fig. 7 One of the metal–ligand hydrogen bonded helices in the structure of **4**.

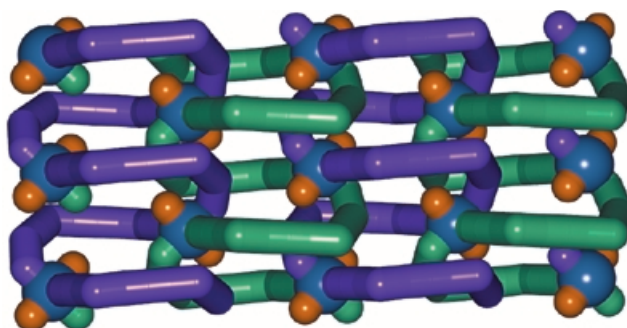


Fig. 8 Schematic representation of the partially interleaved, hydrogen bonded, enantiomeric (green and purple) helices in the structure of **4**.

the coordinated ethanol and the non-coordinated pyridyl nitrogen [ $\text{O}\cdots\text{N}$ ,  $\text{H}\cdots\text{N}$  distances 2.82, 1.94 Å,  $\text{OH}\cdots\text{N}$  angle 165°]. The effect of this hydrogen bonding is the formation of [metal–ligand...metal] helices analogous to those seen in compound **15** (Fig. 7) the helices being propagated by the crystallographic  $2_1$  screw and having a [ligand...H–O–Mn]<sub>2</sub> repeat sequence, the Mn...Mn helix repeat distance being 7.78 Å (*cf.* Cd...Cd 8.24 Å in **15**).

By virtue of the inversion symmetry at Mn, these helices partially interleave (Fig. 8), the non-coordinated pyridyl ring of one helix being sandwiched between the coordinated pyridyl rings of the other and *vice versa*. The pyridyl rings are nearly parallel, being inclined by only 5°, and have centroid–centroid and interplanar spacings of 3.95, 3.87 Å and 3.42, 3.57 Å respectively, indicative of pronounced  $\pi$ – $\pi$  interactions. The only other short intra-helix contact is between the sulfur atom of the isothiocyanate and the  $\text{C}_6\text{F}_4$  ring system, the S–ring centroid distance being 3.81 Å and the S–centroid vector being inclined by 62° to the ring plane. This approach is, to some extent, analogous to those seen for  $\text{X}-\text{C}_6\text{F}_4$  (where X = I, Br or O) in the structures of **6**,  $\{[\text{CuL}(\text{DMF})\text{Br}_2]\cdot(\text{DMF})\}_n$  and **15**.

The combination of the linking of adjacent metal centres *via* H-bonding to form helices and the inversion symmetry at the Mn atom creates sheets of partially interpenetrating helices as illustrated schematically in Fig. 8. Adjacent sheets are stacked such that the  $\text{C}_6\text{F}_4$  rings in one sheet partially overlap their counterparts in the next, the centres of inter-sheet  $\text{C}_6\text{F}_4$  ring systems having a mean inter-planar separation of *ca.* 3.10 Å and a lateral offset of 3.88 Å. Accompanying this arrangement is a  $\text{CF}\cdots\text{C}'\text{F}'$  distance of 3.14 Å.

It should be stressed that the network in **4** is not all-covalent, as is the case in **15**, but is a product of a combination of covalent and hydrogen bonding linkages. The resulting 2-D layer network does not involve any true interpenetration and should be classed as having a (4,4) topology.

### Structure of $[\text{MnL}_2(\text{EtOH})_2\text{Br}_2]$ **3**

In the structure of the manganese(II) isothiocyanate complex, **4**, described above we saw the 2,3,5,6-tetrafluoro-1,4-bis(4-pyridylsulfenyl)benzene ligand (L) using its capability to act as both a coordinating and a hydrogen bonding linkage between metal centres. Here in the manganese bromide complex, **3**, it adopts an identical role but in the process forms a structure which, although at the molecular level is very similar, at the supramolecular level is dramatically different.

The geometry at Mn (Fig. 9) is slightly distorted *trans*-octahedral, with *cis*- angles in the range 85.5(3) to 94.7(3)°. The coordination distances are unexceptional though it is noticeable that in **3** the Mn–O(EtOH) distances are slightly shorter than in the isothiocyanate analogue. Although the complex does not have crystallographic inversion symmetry, the disposition and geometries of the ligands with respect to the central metal atom exhibit only marginal departures from a centrosymmetric

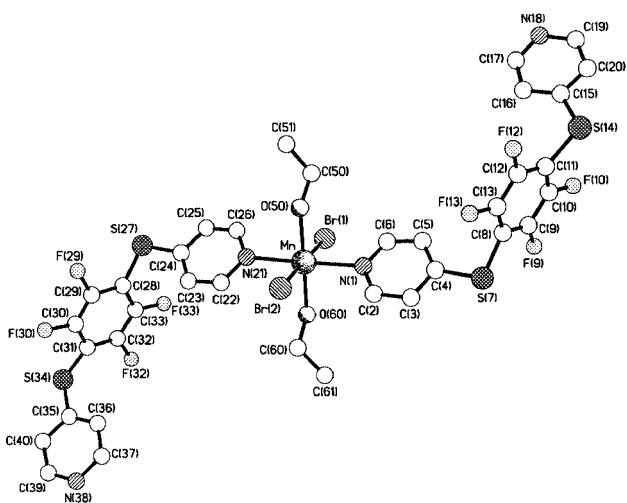


Fig. 9 The manganese coordination environment in the structure of **3**.

arrangement. Both bis(pyridyl) ligands have *syn*-geometries, the pyridyl rings being steeply inclined to the  $\text{C}_6\text{F}_4$  ring systems and with the expected enlargements in the 'interior' C–C–S bond angles (Table 7). There is also a marked bowing of each S– $\text{C}_6\text{F}_4$ –S of *ca.* 18°. The coordinated pyridyl rings are each inclined by *ca.* 55° to the  $\text{MnN}_2\text{O}_2$  plane—a value slightly less than that (67°) seen in the isothiocyanate complex.

As mentioned above, adjacent metal centres are linked indirectly *via* hydrogen bonding between coordinated ethanol molecules and the non-coordinated pyridyl rings. However the geometry of the resulting supramolecular array, although again a (4,4) net, is very different from that observed in the isothiocyanate. In the bromide, corrugated sheets of the type shown in Fig. 10 are formed, comprising hydrogen bonded macrocycles made up from four Mn centres and four bis(pyridyl) ligands. Each of these macrocycles has appreciable free pathways through their centres and these spaces are effectively totally filled *via* a system of triply interpenetrating (4,4) nets. This complex weave, in which the interpenetration is of the 'over 2-under 2' type, is illustrated schematically in Fig. 11, where the three colours represent the three component (4,4) nets. Within each sheet there are C–H... $\pi$  edge-to-face interactions between the edge of the hydrogen bonded pyridyl rings and the faces of their coordinated counterparts, with H... $\pi$  distances of 2.81 and 2.91 Å to the respective ring centres. [A structure comprising interweaving of three independent (4,4) nets has recently been reported for the compound bis{3-[2-(4-pyridyl)ethenyl]benzoato}cadmium.<sup>5</sup>]

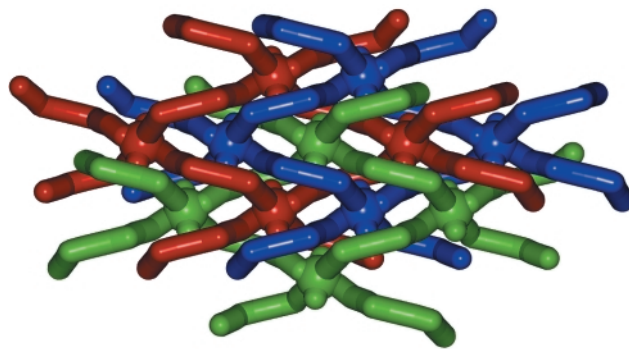


Fig. 11 Schematic representation of part of one of the triply interwoven sheets in **3**.

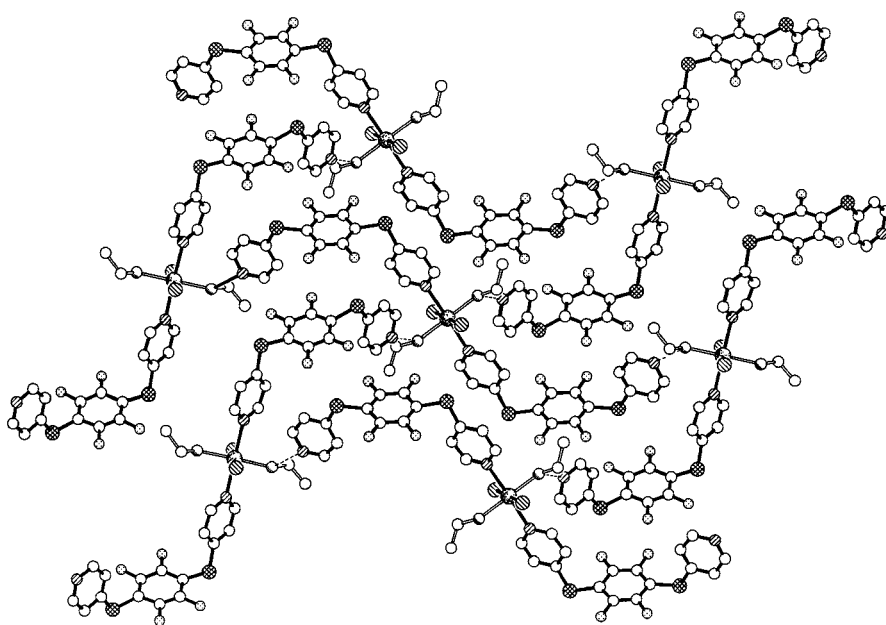
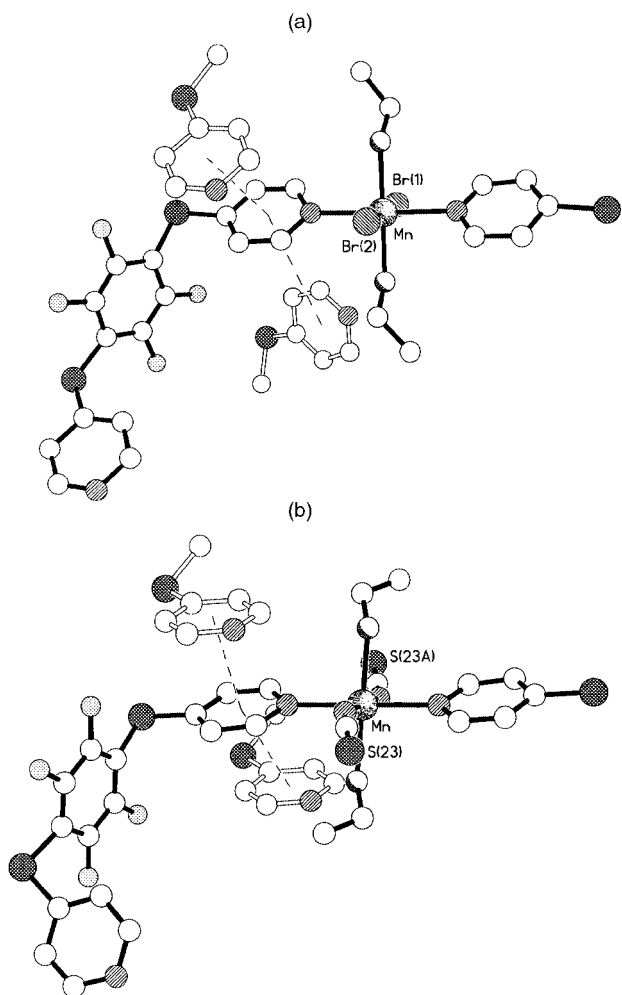


Fig. 10 Part of one of the continuous corrugated hydrogen bonded sheets in the structure of **3**.



**Fig. 12** A comparison of the intermolecular approaches of the non-coordinated pyridyl rings to the coordinated rings in: (a) the structure of compound **3**; (b) the structure of compound **4**.

The 'cement' holding the interpenetrating nets together is principally face-to-face  $\pi$ - $\pi$  stacking between the non-coordinated pyridyl rings in one net and a coordinated pyridyl ring in the next [centroid-centroid and interplanar spacings of 3.58 and 3.38 Å, rings inclined by 3° for one set and 3.58 and 3.43 Å and 6° for the other]. Thus, in this structure, the coordinated pyridyl ring has non-coordinated pyridyl rings approaching, in one instance in a face-to-face geometry, and in the other in an edge-to-face arrangement (*cf.* the twin face-to-face approach in **4**) (Fig. 12).

There is also a much weaker  $\text{Br} \cdots \text{C}_6\text{F}_4$  inter-weave approach of the bromine atoms in one network and the  $\text{C}_6\text{F}_4$  ring system of another of 4.01 and 3.95 Å respectively. These electrostatic interactions are directly analogous to, though much weaker than, the other  $\text{X} \cdots \text{C}_6\text{F}_4$  ( $\text{X} = \text{Br}, \text{I}, \text{O}$ ) interactions discussed previously. [A detailed analysis of the geometries of approach of halides, oxygens and sulfur atoms to the centroids of  $\text{C}_6\text{F}_4$  ring systems and to their ring planes indicates that a correlation exists between the approach distance and the atom  $\cdots$  ring-centroid vector for all the species investigated.<sup>9</sup>]

The question immediately posed is why the network seen for  $[\text{MnL}_2(\text{EtOH})_2\text{Br}_2]$  is so different from that seen in the isothiocyanate analogue when both the conformation of the coordination geometry at the metal centre of the complex and the hydrogen bonding are so similar? The key appears to be in the geometry of approach of the non-coordinated pyridyl ring to the oxygen atom of the ethanol ligand in each structure. In the isothiocyanate complex the hydrogen bonding between adjacent complexes is supplemented by face-to-face  $\pi$ - $\pi$  stack-

ing between the hydrogen bonded pyridyl ring in one and the coordinated pyridyl ring in the next. In the bromide the van der Waals radius of the bromine atom inhibits such an approach from both faces; instead, the hydrogen bonding interaction is again supplemented but this time by an edge-to-face  $\text{CH} \cdots \pi$  interaction (2.81 Å) between the same pair of ring systems.

#### Other complexes and spectroscopic studies

The solid state electronic spectrum of the cobalt iodide complex, **6**, shows the strong bands [5700sh, 6800, 9090  $\text{cm}^{-1}$ , components of  ${}^4\text{T}_1(\text{F})$ , multicomponent band centred at 15150,  ${}^4\text{T}_1(\text{P})$ ] characteristic<sup>10</sup> of the distorted tetrahedral coordination geometry found from the X-ray study. The cobalt chloride complex, **5**, has the same type of electronic reflectance spectrum, with strong bands at 6250, 7140sh, 9520, 16400, 17250sh  $\text{cm}^{-1}$ , again indicating an essentially tetrahedral geometry at the cobalt centres. Consistent with this<sup>11</sup> is the observation of  $\nu(\text{Co}-\text{Cl})$  IR bands at 302 and 349  $\text{cm}^{-1}$ . Whilst it appears evident from these observations that the metal ion coordination geometry in compound **5** is essentially the same as in its cobalt(II) iodide analogue **6**, the X-ray powder patterns of the two compounds differ. An analogous chain structure but with different packing is quite likely, but alternative structures, *e.g.* large ring formation,<sup>12</sup> are possible for cobalt(II) tetrahedrally coordinated to extended reach ligands.

X-Ray powder diffraction studies show that the zinc compounds  $\text{ZnLX}_2$  ( $\text{X} = \text{Cl}$  **8**, **10**) form essentially isomorphous pairs with their respective cobalt(II) analogues, though with differences in the relative intensities of some of the diffraction peaks, mainly at higher angles. An essentially tetrahedral geometry at the zinc atom in  $\text{ZnLCl}_2$  **8** is also indicated by  $\nu(\text{Zn}-\text{Cl})$  IR bands at 295 and 331  $\text{cm}^{-1}$  (with corresponding bands at 294 and 333  $\text{cm}^{-1}$  in the solid state Raman spectrum).

In contrast to the cobalt(II) complexes discussed above, the solid state electronic spectrum of  $\text{NiLCl}_2$ , **7**, comprises relatively low intensity bands at 5900sh, 8600, 14300, 22200sh and 24300  $\text{cm}^{-1}$  characteristic<sup>13</sup> of a polymeric array of six-coordinate nickel(II) centres, produced by a combination of chloride bridges and pairs of *trans*-disposed pyridine units, as in  $\text{Ni}(\text{py})_2\text{Cl}_2$ . In the case of compound **7**, the organic bis-(pyridyl) ligand connecting the chloride bridged chains of metal centres is sufficiently long that it is likely that there is some form of mutual strand interweaving of the general type observed for the manganese(II) bromide complex, compound **3**, discussed above, so as to minimise 'void' space. We were, however, unable to obtain this compound in good crystalline form to determine its true long-range structure so as to verify this.

Attempts to grow X-ray quality crystals of a manganese(II) chloride complex were also unsuccessful. Variation of the experimental conditions, in attempts to induce crystal formation, afforded complexes of two different stoichiometries  $\text{MnLCl}_2$ , **1**, and  $\text{MnL}_2\text{Cl}_2$ , **2**, neither of which contains the ethanol molecules that proved to be so important in the structures formed by the other manganese complexes, compounds **3** and **4**.

The X-band EPR spectrum of compound **1** in the solid state has just one broad band centred at  $g_{\text{eff}} = 2$  indicating strong dipolar coupling between the manganese centres and the presence of a polymeric structure involving chloride bridges, as in *e.g.*  $\text{Mn}(\text{py})_2\text{Cl}_2$ .<sup>14</sup> The X-ray powder patterns of  $\text{MLCl}_2$  ( $\text{M} = \text{Mn}$  **1**, **Cd** **12**) show very marked similarities in the patterns of their principal lines, even to high angles, and although there is not a sufficient match to establish strict isomorphism it seems likely that the two compounds have basically the same type of polymeric structure. Accordingly we prepared Mn-doped samples of  $\text{CdLCl}_2$  (nominal 1% Mn doping) to investigate the EPR spectrum of the Mn centre in this type of polymeric array without the effects of the magnetic concentration present in 'normal' samples of  $\text{MnLCl}_2$ .

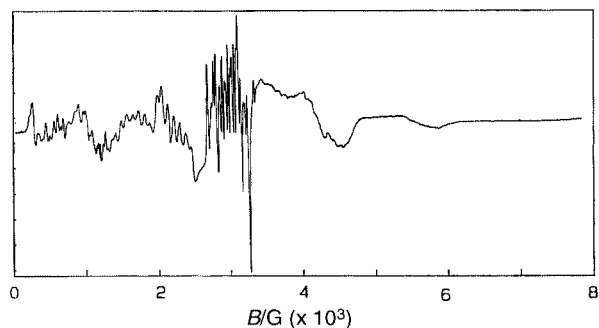


Fig. 13 Room temperature X-band EPR spectrum of a powdered sample of compound **12** 'doped' with 1% (nominal) Mn(II).

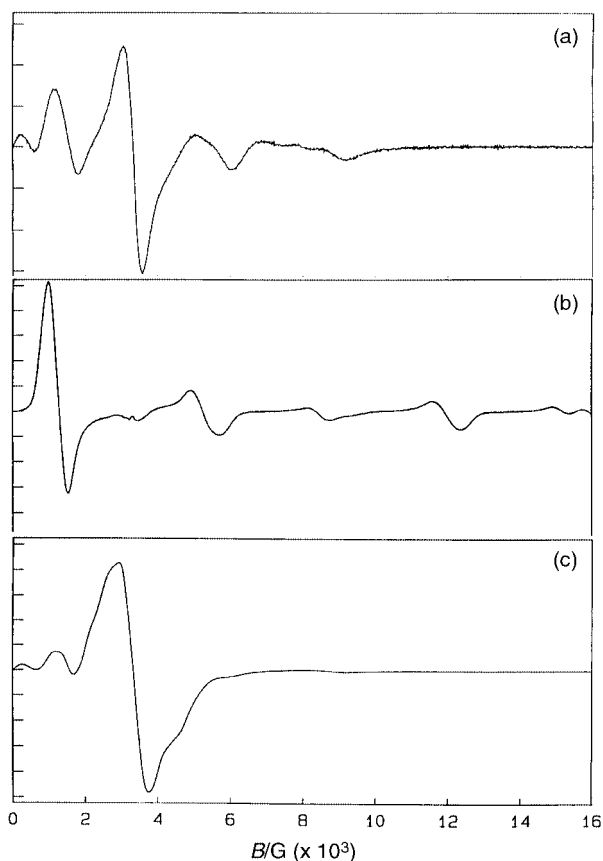


Fig. 14 Room temperature X-band EPR spectra of powdered samples of: (a) compound **2**; (b) compound **3**; (c) compound **4**.

The resulting spectrum (Fig. 13) shows the complex band system, principally at low magnetic fields, due to the zero-field splitting (zfs) arising from the lower than cubic symmetry of the metal environment, with additional band splittings from the manganese nuclear hyperfine coupling. This spectrum is of the same type as those observed for manganese(II) ions doped into halide-bridged polymeric complexes  $\text{CdL}''_2\text{Cl}_2$  (where  $\text{L}'' = \text{pyridine}$  or a substituted pyridine).<sup>15</sup>

The X-band EPR spectrum of  $\text{MnL}_2\text{Cl}_2$  (compound **2**) in the solid state (Fig. 14a) is, however, dramatically different from that of **1**. Even as the 'pure' (non-diluted) compound it shows the complex band system from the effects of zfs thus indicating the absence of chloride bridges. Indeed, the spectrum is of the general type observed for six-coordinate compounds of the type  $\text{MnL}''_4\text{Cl}_2$  (where  $\text{L}'' = \text{pyridine}$  or a substituted pyridine).<sup>16</sup> From the stoichiometry of the complex it appears that, in this case, both pyridine units of the organic ligand are bonded to the manganese centres, but, because of the length of the organic bridges thus formed, there is sufficient magnetic

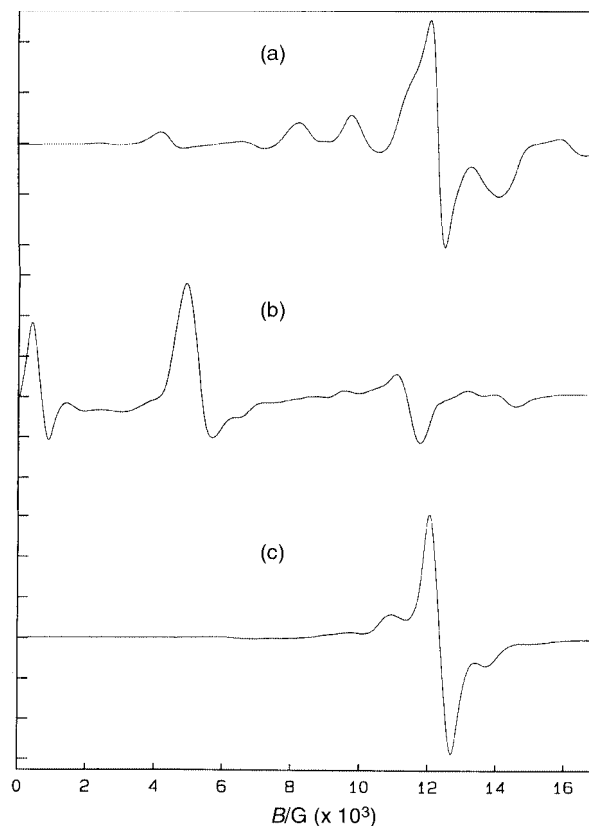


Fig. 15 Room temperature Q-band EPR spectra of powdered samples of: (a) compound **2**; (b) compound **3**; (c) compound **4**.

dilution to permit the observation of the effects of the zfs. The form of the X-band spectrum, both in terms of band positions and relative intensities,<sup>16</sup> indicates that the manganese coordination environment has very close to axial symmetry and with a value of the zfs parameter  $D$  in the range  $0.15\text{--}0.2\text{ cm}^{-1}$ . The same conclusions can be drawn from the EPR spectrum at Q-band frequency (Fig. 15a).

The X-band spectra of solid samples of  $[\text{MnL}_2(\text{EtOH})_2\text{Br}_2]$ , **3**, and  $[\text{MnL}_2(\text{EtOH})_2(\text{NCS})_2]$ , **4**, are shown in Figs. 14b and 14c respectively, and their Q-band spectra are shown in Figs. 15b and 15c respectively. The X-ray studies have shown that in each case the metal centres have distorted octahedral coordination geometry. In both compounds there are three *trans*-disposed pairs of different donor groups resulting in a rhombic arrangement of ligands; that, in turn, results in EPR spectra showing pronounced zfs. Although, in strictly geometric terms, the metal coordination geometries of **3** and **4** are very similar, the change in anion from Br to NCS has a major effect on the respective EPR spectra. In the case of the bromide the X-band spectrum (Fig. 14b) is dominated by a strong band at *ca.* 1260 G but with other bands extending out to near 16000 G (the limit of the range studied) and the Q-band spectrum (Fig. 15b) also shows a very wide range of band positions. In the case of the isothiocyanate complex, however, the main absorption is near  $g_{\text{eff}} = 2$  and the spread of zfs components is very much less. These differences reflect, of course, the much weaker crystal field generated by the bromide ions as compared with the pyridine units of the organic ligand and the N-bonded isothiocyanate ions and thereby a significantly larger value of the zfs parameter  $D$  in the case of compound **3**.

## Conclusion

The principal feature arising from the results described here, together with those we previously reported for Cu(II),<sup>6</sup> is the dramatic diversity of solid state structures obtained by varying



both the metal ion, the counter anions and the reaction conditions. The effects of the metal ion variation are relatively easy to rationalise on the basis of the preferred coordination geometries of the metal ions involved. The ways in which the geometric arrays propagate from those coordination centres appear, however, to depend on a complex interplay of a set of variable factors, which include the nature of the anions, the conformations adopted by the extended bis(pyridyl) ligand, the effects of  $\pi$ - $\pi$  interactions, the involvement of dipolar interactions between coordinated anions and the  $-C_6F_4-$  spacer unit, and hydrogen bonding interactions involving coordinated solvent molecules. The consequence is that, whilst a careful examination of the structure adopted may permit a rationalisation of those, and other, factors involved, the structures are currently not readily amenable to confident prediction.

The situation is well illustrated by the structures observed for compounds  $[MnL_2(EtOH)_2Br_2]$ , **3**, and  $[MnL_2(EtOH)_2(NCS)_2]$ , **4**, where there are major differences in the long range arrays extending from what are very similar coordination geometries at the Mn centres. In both compounds hydrogen bonding between the coordinated ethanol molecules and the non-coordinated pyridyl rings plays an important role. As set out in the detailed discussion of the structures, in the isothiocyanate complex **4** this hydrogen bonding is supplemented by face-to-face  $\pi$ - $\pi$  stacking, an interaction which is, however, inhibited by the size of the coordinated bromine atom in the case of compound **3** and that, in turn, results in a quite different array structure.

In recent years various types of polymeric structures based on spacer-linked bis(4-pyridyl) donor units have been reported<sup>2-5</sup> with the evident aim of providing the fundamental information needed if accurate prediction of structure type is to be achieved. The results we report here clearly indicate that this will be, at best, a long term goal because of the evident complexity and diversity of the various factors involved.

## Acknowledgements

We thank the EPSRC for Research Studentships (to D. A. G. and S. H.) and for the diffractometer, the University of London Intercollegiate Research Service for the Raman equipment and Dr Frank Mabbs and Dr Eric McInnes of the EPSRC.cw.EPR Service Centre, University of Manchester for EPR measurements.

## References

- R. Robson, B. F. Abrahams, S. R. Batten, R. W. Gable, B. F. Hoskins and J. Liu, *Supramolecular Architecture*, ACS publications, Washington, DC, 1992, ch. 19; M. J. Zaworotko, *Chem. Soc. Rev.*, 1994, 283; C. A. Hunter, *Angew. Chem., Int. Ed. Engl.*, 1995, **34**, 1079; C. L. Bowes and G. A. Ozin, *Adv. Mater.*, 1996, **8**, 13; M. Fujita and K. Ogura, *Bull. Chem. Soc. Jpn.*, 1996, **69**, 1471; M. Munakata, L. P. Wu and T. Kuroda-Sowa, *Bull. Chem. Soc. Jpn.*, 1997, **70**, 1727; C. Janiak, *Angew. Chem., Int. Ed. Engl.*, 1997, **36**, 1431; S. R. Batten and R. Robson, *Angew. Chem., Int. Ed.*, 1998, **37**, 1460; A. J. Blake, N. R. Champness, P. Hubberstey, W.-S. Li, M. A. Withersby and M. Schröder, *Coord. Chem. Rev.*, 1999, **183**, 117.
- R. W. Gable, B. F. Hoskins and R. Robson, *J. Chem. Soc., Chem. Commun.*, 1990, 1677; M. Fujita, J. Yazaki and K. Ogura, *J. Am. Chem. Soc.*, 1990, **112**, 5645; P. J. Stang and V. V. Zhdankin, *J. Am. Chem. Soc.*, 1993, **115**, 9808; M. Fujita, Y. J. Kwon, S. Washizu and K. Ogura, *J. Am. Chem. Soc.*, 1994, **116**, 1151; P. J. Stang and D. H. Cao, *J. Am. Chem. Soc.*, 1994, **116**, 4981; L. R. MacGillivray, S. Subramanian and M. J. Zaworotko, *J. Chem. Soc., Chem. Commun.*, 1994, 1325; S. R. Batten, B. F. Hoskins and R. Robson, *J. Am. Chem. Soc.*, 1995, **117**, 5385; P. J. Stang, D. H. Cao, S. Saito and A. M. Arif, *J. Am. Chem. Soc.*, 1995, **117**, 6273; F. Robinson and M. J. Zaworotko, *J. Chem. Soc., Chem. Commun.*, 1995, 2413; S. Subramanian and M. J. Zaworotko, *Angew. Chem., Int. Ed. Engl.*, 1995, **34**, 2127; P. Losier and M. J. Zaworotko, *Angew. Chem., Int. Ed. Engl.*, 1996, **35**, 2779; A. S. Batsanov, M. J. Begley, P. Hubberstey and J. Stroud, *J. Chem. Soc., Dalton Trans.*, 1996, 1947; A. J. Blake, S. J. Hill, P. Hubberstey and W.-S. Li, *J. Chem. Soc., Dalton Trans.*, 1997, 913; L. Carlucci, G. Ciani, D. M. Proserpio and A. Sironi, *J. Chem. Soc., Dalton Trans.*, 1997, 1801; J. Li, H. Zeng, J. Chen, Q. Wang and X. Wu, *Chem. Commun.*, 1997, 1213; J. Lu, T. Paliwala, S. C. Lim, C. Yu, T. Niu and A. J. Jacobson, *Inorg. Chem.*, 1997, **36**, 923; B. Olenyuk, A. Fechtenkötter and P. J. Stang, *J. Chem. Soc., Dalton Trans.*, 1998, 1707; M.-L. Tong, X.-M. Chen, X.-L. Yu and T. W. C. Mak, *J. Chem. Soc., Dalton Trans.*, 1998, 5; M.-L. Tong, B.-H. Ye, J.-W. Cai, X.-M. Chen and S. W. Ng, *Inorg. Chem.*, 1998, **37**, 2645; L. R. MacGillivray, R. H. Groeneman and J. L. Atwood, *J. Am. Chem. Soc.*, 1998, **120**, 2676; Y. Zhang, L. Jianmin, D. Wei, M. Nishiura and T. Imamoto, *Chem. Lett.*, 1999, 195; K. Biradha, C. Seward and M. J. Zaworotko, *Angew. Chem., Int. Ed.*, 1999, **38**, 492; Q. Wang, X. Wu, W. Zhang, T. Sheng, X. Wu and J. Li, *Inorg. Chem.*, 1999, **38**, 2223.
- M. Fujita, S. Nagao, M. Iida, K. Ogata and K. Ogura, *J. Am. Chem. Soc.*, 1993, **115**, 1574; M. Fujita, F. Ibukuro, H. Hagihara and K. Ogura, *Nature (London)*, 1994, **367**, 720; M. Fujita, F. Ibukuro, K. Yamaguchi and K. Ogura, *J. Am. Chem. Soc.*, 1995, **117**, 4175; J. A. Real, E. Andrés, M. C. Munoz, M. Julve, T. Granier, A. Bousseksou and F. Varret, *Science*, 1995, **268**, 265; M. Fujita, O. Sasaki, T. Mitsuhashi, T. Fujita, J. Yazaki, K. Yamaguchi and K. Ogura, *Chem. Commun.*, 1996, 1535; T. L. Henniger, D. C. MacQuarrie, P. Losier, R. D. Rogers and M. J. Zaworotko, *Angew. Chem., Int. Ed. Engl.*, 1997, **36**, 972; A. J. Blake, N. R. Champness, S. S. M. Chung, W.-S. Li and M. Schröder, *Chem. Commun.*, 1997, 1005; A. J. Blake, N. R. Champness, S. S. M. Chung, W.-S. Li and M. Schröder, *Chem. Commun.*, 1997, 1675; A. J. Blake, N. R. Champness, A. Khlobystov, D. A. Lemenovskii, W.-S. Li and M. Schröder, *Chem. Commun.*, 1997, 2027; L. Carlucci, G. Ciani, D. W. v. Gudenberg and D. M. Proserpio, *Inorg. Chem.*, 1997, **36**, 3812; M. Fujita, M. Aoyagi and K. Ogura, *Bull. Chem. Soc. Jpn.*, 1998, **71**, 1799; L. Carlucci, G. Ciani, P. Macchi and D. M. Proserpio, *Chem. Commun.*, 1998, 1837; F. D. Rochon, M. Andruh and R. Melanson, *Can. J. Chem.*, 1998, **76**, 1564; L. Carlucci, G. Ciani and D. M. Proserpio, *Chem. Commun.*, 1999, 449; S. Noro, M. Kondo, T. Ishii, S. Kitagawa and H. Matsuzaka, *J. Chem. Soc., Dalton Trans.*, 1999, 1569; M. Kondo, M. Shimamura, S. Noro, T. Yoshitomi, S. Minakoshi and S. Kitagawa, *Chem. Lett.*, 1999, 285.
- M. Fujita, Y. J. Kwon, O. Sasaki, K. Yamaguchi and K. Ogura, *J. Am. Chem. Soc.*, 1995, **117**, 7287.
- W. Lin, O. R. Evans, R.-G. Xiong and Z. Wang, *J. Am. Chem. Soc.*, 1998, **120**, 13272.
- D. M. L. Goodgame, D. A. Grachvogel, M. A. Hitchman, N. J. Long, H. Stratemeier, A. J. P. White, J. L. M. Wicks and D. J. Williams, *Inorg. Chem.*, 1998, **37**, 6354.
- SHELXTL PC version 5.03, Siemens Analytical X-Ray Instruments, Inc., Madison, WI, 1994.
- H. M. Colquhoun, C. J. O'Mahoney and D. J. Williams, *Polymer*, 1993, **34**, 218.
- D. M. L. Goodgame, D. A. Grachvogel and D. J. Williams, in preparation.
- A. B. P. Lever, *Inorganic Electronic Spectroscopy*, Elsevier, Amsterdam, 2nd edn., 1984, pp. 496-503.
- R. J. H. Clark and C. S. Williams, *Inorg. Chem.*, 1965, **4**, 350.
- Z. Atherton, D. M. L. Goodgame, S. Menzer and D. J. Williams, *Inorg. Chem.*, 1998, **37**, 849.
- D. M. L. Goodgame, M. Goodgame and M. J. Weeks, *J. Chem. Soc.*, 1964, 5194.
- R. D. Dowsing, J. F. Gibson, D. M. L. Goodgame, M. Goodgame and P. J. Hayward, *Nature (London)*, 1968, **219**, 1037.
- M. Goodgame and J. N. Okey, *Inorg. Chim. Acta*, 1985, **103**, 67.
- R. D. Dowsing, J. F. Gibson, M. Goodgame and P. J. Hayward, *J. Chem. Soc. A*, 1969, 187.